RESEARCH ARTICLE
SPACE PHYSICS: MAGNETOSPHERIC PHYSICS

Earth and Planetary Physics
6: 546–554, 2022
doi: 10.26464/epp2023003

Validation of the use of THEMIS-B and THEMIS-C as a near-Earth solar wind monitor

DianJun Zhang[1,2], WenLong Liu[1,2*], and Zhao Zhang[1,2]

[1]School of Space and Environment, Beihang University, Beijing 100191, China;

[2]Key Laboratory of Space Environment Monitoring and Information Processing, Ministry of Industry and Information Technology, Beijing 100191, China

Key Points:

- We systematically compare THEMIS-B and C measurements in near-Earth space with solar wind measurements obtained from the L1 point.
- Differences between two datasets suggest possible variation in the solar wind environment while propagating from the L1 point to near-Earth space.
- We suggest that THEMIS-B and THEMIS-C are alternative monitors of the near-Earth solar wind environment.

Citation: Zhang, D. J., Liu, W. L., and Zhang, Z. (2022). Validation of the use of THEMIS-B and THEMIS-C as a near-Earth solar wind monitor. *Earth Planet. Phys.*, *6*(6), 546–554. http://doi.org/10.26464/epp2023003

Abstract: Two THEMIS (Time History of Events and Macroscale Interactions during Substorms) spacecraft, B and C, began orbiting the Moon in 2011 and have since provided routine measurements of the plasma conditions in the lunar orbit. In this study, we systematically compare these measurements in near-Earth space with solar wind measurements obtained from the Lagrangian 1 (L1) point and propagated to the Earth, including measurements in the OMNI database and from the Wind spacecraft. A statistical comparison between THEMIS data and data from the OMNI database from September 2011 to December 2017 showed that the *Y* and *Z* components of the magnetic field and the flow speed are generally consistent between the two data sets. The ion number density and the dynamic pressure measured by THEMIS in near-Earth space are lower than those in the OMNI database, suggesting possible variation in the solar wind environment while propagating from the L1 point to near-Earth space. We further show two examples in which near-Earth solar wind measurements are applied in calculating the magnetopause location and in quantifying the magnetic field response to interplanetary shocks. Both examples suggest that using solar wind data from near-Earth space achieves better results than using solar wind data from the L1 point. These results provide validation of THEMIS-B and THEMIS-C as an alternative monitor of the near-Earth solar wind environment.

Keywords: interplanetary shocks; solar wind; magnetosphere

1. Introduction

The interaction between the solar wind and magnetosphere controls the energy and mass transport to the magnetosphere and subsequently affects dynamic phenomena in the magnetosphere, such as magnetic storms, substorms, and auroral activity (Cao JB et al., 2008, 2010; Wei Y et al., 2008, 2009; Liu WL et al., 2009, 2010; Yu YQ and Ridley, 2011; Fu HS et al., 2012, 2013; Li LY et al., 2016; Yu YQ et al., 2017).

Solar wind parameters, such as the magnetic field and solar wind density, velocity, and dynamic pressure, are critical factors in investigating the solar wind–magnetosphere interaction. For example, an enhancement of the solar wind dynamic pressure can produce compression of the Earth's magnetosphere, leading to an increase in the global magnetic field (Wang C et al., 2009, 2010; Yue C et al., 2010; Zhang DJ et al., 2018). This may further drive a geomagnetic storm in the Earth's magnetosphere (Borovsky and Denton, 2006; Shen XC et al., 2017). The energy from the solar wind may be transferred into the Earth's magnetosphere in several ways, such as through ultralow-frequency (ULF) wave excitations (Zhang XY et al., 2010; Liu WL et al., 2013, 2016; Shen XC et al., 2015; Wang CR et al., 2015; Korotova et al., 2018; Zhang DJ et al., 2020), the acceleration and transport enhancement of energetic particles (Li XL et al., 1993; Zong QG et al., 2009; Foster et al., 2015; Kanekal et al., 2016; Liu ZY et al., 2017; Liu Y et al., 2019; Patel et al., 2019; Xiong Y et al., 2021; Tang CL et al., 2022), and the aurora in the polar region (Zhou XY and Tsurutani, 1999; Zhou XY et al., 2017; Zhu MH et al., 2022).

In most studies investigating the solar–terrestrial interaction, monitoring of the signature of the solar wind environment has been based on spacecraft measurements at the Sun–Earth Lagrangian 1 (L1) point, such as by IMP-8 (International Monitoring Platform-8), ACE (Advanced Composition Explorer), and Wind

Correspondence to: W. L. Liu, liuwenlong@buaa.edu.cn
Received 22 AUG 2022; Accepted 08 SEP 2022.
Accepted article online 26 SEP 2022.

spacecraft, which have been ensembled into the OMNI database. For example, Russell et al. (1994) examined the response of the low-latitude *H* component of the Earth's magnetic field during the passage of interplanetary shocks with IMP-8 measurements. However, propagation is necessary to correlate the solar wind measurement at the L1 point and its response in the magnetosphere. The time delay of propagation is dependent on the velocity and structures of the solar wind at a scale of tens of minutes, with an error as large as 10 minutes. Studies have also been done using measurements of Earth-orbiting spacecraft, such as Cluster, THEMIS (Time History of Events and Macroscale Interactions during Substorms), and MMS (Magnetospheric Multiscale), to monitor the solar wind when the craft is outside the bow shock. However, the opportunity to gather such solar wind measurements is limited by the time during which the spacecraft is located in the solar wind because these missions are designed to observe the magnetosphere.

In contrast, in previous studies on the radial characteristic of the solar wind property in the heliosphere, the spatial interval was generally beyond 0.1 AU; thus, the L1 point and the near-Earth space are usually considered the same location rather than two different locations (Richardson et al., 1995; Bruno et al., 2003). Therefore, the difference in the solar wind measurement between the L1 point and near-Earth space has rarely been investigated.

In this study, taking advantage of the THEMIS mission, which sent two probes to the lunar orbit that stay predominantly in the solar wind, we perform a systematic comparison between the solar wind parameter measured at the L1 point and in near-Earth space. Our results provide validation of the THEMIS measurements as an alternative monitor of the near-Earth solar wind environment.

2. Data Sets

Measurements of the near-Earth solar wind were obtained from THEMIS probes B and C (hereafter referred to as TH-B and TH-C; Angelopoulos et al., 2008). After the THEMIS mission was extended in early 2010, the orbits of the two probes were transferred to a lunar orbit and were named the ARTEMIS (Acceleration, Reconnection, Turbulence, and Electrodynamics of the Moon's Interaction with the Sun) probes P1 and P2 (Angelopoulos, 2011). The magnetic field measurements were obtained by the fluxgate magnetometer instrument (Auster et al., 2008), and plasma measurements were obtained by the electrostatic analyzer instrument (McFadden et al., 2008).

In this study, TH-B and TH-C data from September 2011 to December 2017 are analyzed with its distribution in the Geocentric Solar Magnetospheric coordinate system shown in Figure 1. Both TH-B and TH-C are at distances of ~50–65 R_E from the Earth. Because the Moon orbits the Earth in a period of ~30 days, TH-B and TH-C periodically enter the magnetotail and solar wind. Thus, we first limit the time range to the interval when both TH-B and TH-C are located at least 5 R_E outside the bow shock to guarantee that the data used in this study were measured in the solar wind. In addition, both TH-B and TH-C may pass the lunar wake, where the plasma can be greatly deflected from the solar wind, which also must be excluded from our study. In previous studies, the lunar wake was identified by a depletion of the ion density ($N_{wake}/N_{sw} < 0.8$) or an acceleration or deceleration of the plasma velocity ($||V_{wake}| - |V_{sw}|| > 50$ km/s; e.g., Zhang H et al., 2014), where the subscripts "wake" and "sw," respectively, represent the lunar wake and solar wind plasma. Thus, we exclude the time interval when $N_i/N_{bg} < 0.7$ and $||V_i| - |V_{bg}|| > 50$ km/s, where N_i and V_i are the real-time-measured ion density and velocity, respectively, and N_{bg} and V_{bg} are the 6-hour-averaged background data of N_i and V_i. A 6-hour-average window is sufficient for this study because it usually takes 1 hour for TH-B and TH-C to pass through the region of the lunar wake (e.g., Halekas et al., 2011). The spatial distributions of data coverage of TH-B and TH-C are presented in the left and right panels of Figure 1, respectively, and are indicated by color. In this study, the total coverage of TH-B is 18,218 hours, and that of TH-C is 17,745 hours.

The solar wind data set obtained from the OMNI database, which was originally obtained by the spacecraft at the L1 point and time-shifted to the nose of the Earth's bow shock (Weimer and King,

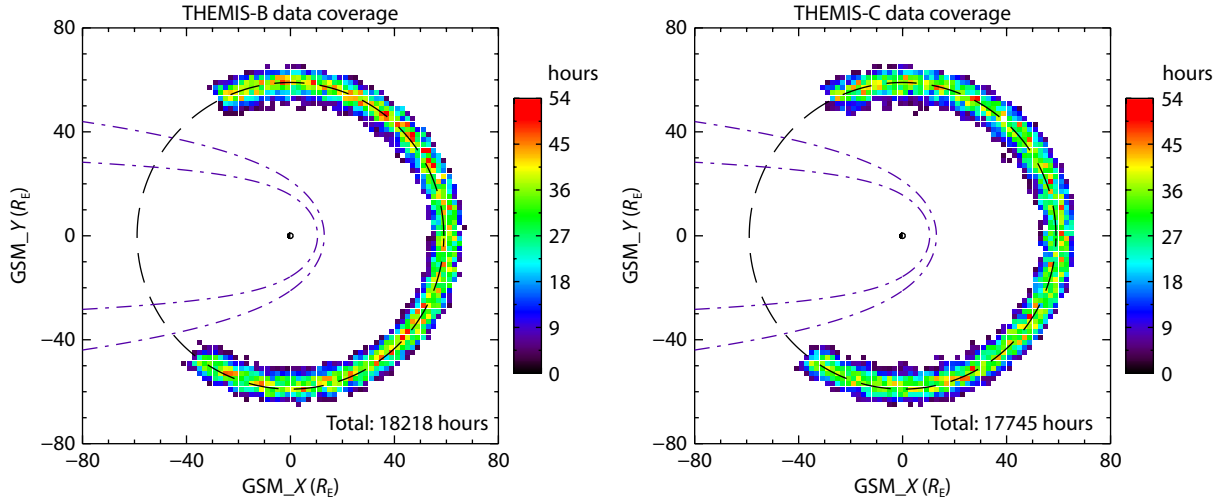

Figure 1. Orbit plot and data coverage of THEMIS (TH)-B (left) and TH-C (right) in the solar wind during the period from September 2011 to December 2017.

2008), is used in the study for comparison with THEMIS observations. The solar wind data obtained from the Wind spacecraft with a higher time resolution are also used in this study. Magnetic field measurements are from the magnetic field instrument (Lepping et al., 1995), and the plasma investigation is from the solar wind experiment (Ogilvie et al., 1995).

3. Comparison Between the Solar Wind Measurements at Near-Earth Space and the L1 Point

3.1 Observation of an Interplanetary Shock Event

In Figure 2, we present a sample of the comparison between the OMNI database and THEMIS measurements on August 31, 2017.

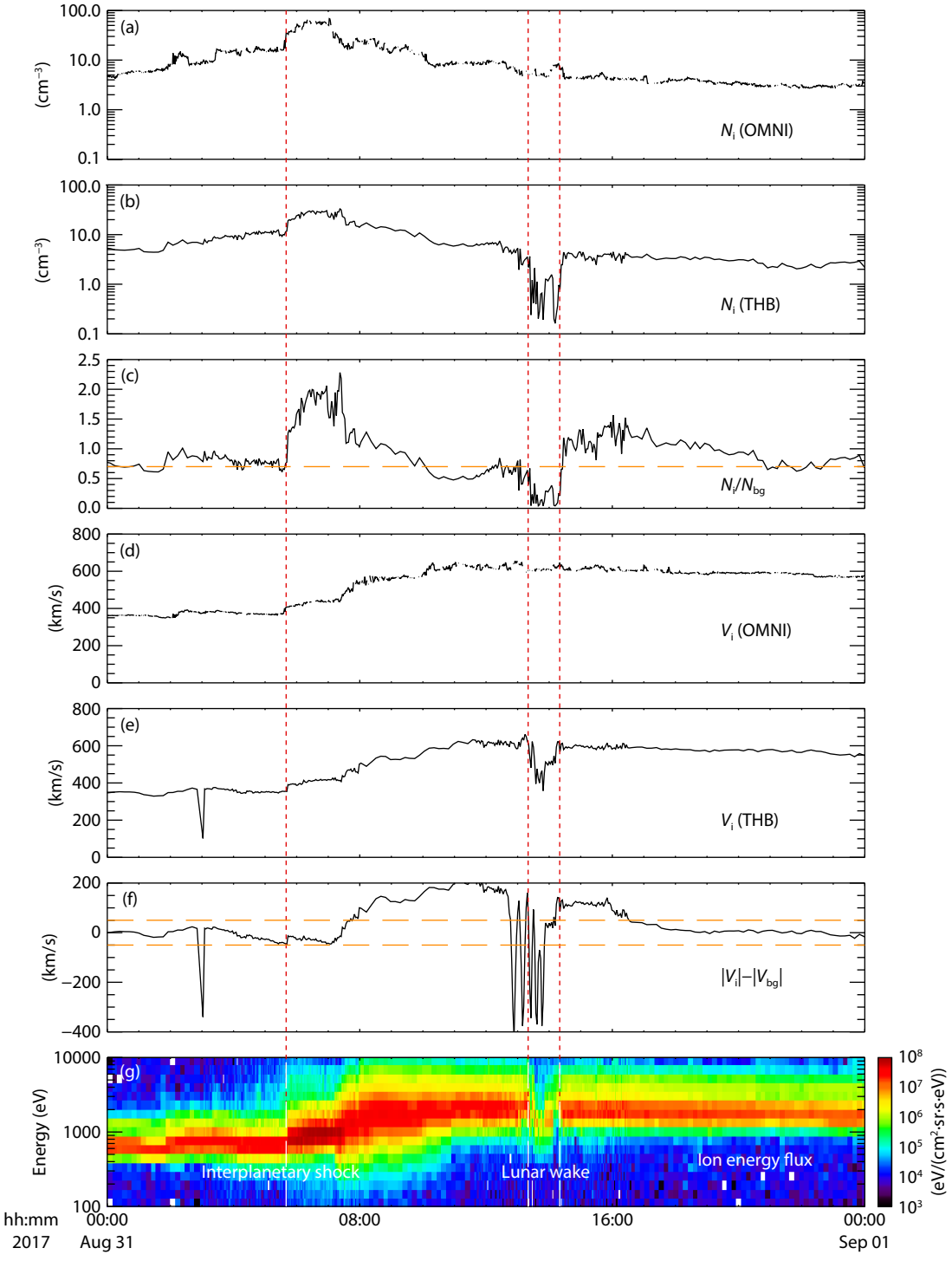

Figure 2. Daily plot of OMNI and THEMIS (TH)-B data on August 31, 2017. (a–b) Ion density N_i from OMNI data and TH-B measurements; (c) the value of N_i/N_{bg}, with a threshold value of 0.7, marked by the orange dashed line, for the identification of the lunar wake; (d–e) flow speed V_i from OMNI data and TH-B measurements; (f) the value of $|V_i| - |V_{bg}|$, with a threshold of $||V_i| - |V_{bg}|| > 50$ km/s, marked by the orange dashed lines, for the identification of the lunar wake; (g) energy flux spectrum of electrons measured by TH-B. Vertical dashed lines indicate the encounter of an interplanetary shock and the passage of the lunar wake.

An interplanetary shock, indicated by enhancements of the ion density and flow speed shown in Figure 2, was observed around 05:40 universal time (UT) by both OMNI and TH-B. The evolution of ion density (Figures 2a and 2b for OMNI and TH-B, respectively) and flow speed (Figures 2d and 2e for OMNI and TH-B, respectively) are very similar, suggesting the two data sets are highly consistent. Note that at 05:38 UT, the amplitude of ion density enhancement in the OMNI data is 19 cm^{-3} (16–35 cm^{-3}), whereas at 05:44 UT in TH-B, it is 10 cm^{-3} (9.8–19.8 cm^{-3}). At the same time, the amplitude of the flow speed enhancement in the OMNI data is 40 km/s (372–412 km/s), whereas in TH-B, it is 41 km/s (354–395 km/s). This result suggests that the dynamic pressure measured by the TH-B spacecraft at the near-Earth region tends to be lower than that in the OMNI database measured at the L1 point.

In the spectral plot of ion energy flux observed by TH-B presented in Figure 2g, the successive spectral peaks at ~800–2,000 eV suggest that TH-B was mostly located in the environment of the solar wind except for the interval from 13:20 to 14:20 UT, in which the gap in the peak spectrum indicates the passage of a lunar wake. Simultaneously, a great depletion of ion density (minimum $N_i < 0.1$ cm^{-3}) and flow speed (minimum V_i ~400 km/s) for approximately 1 hour observed by TH-B also indicates the passage of the lunar wake, as shown in Figures 2b and 2e. As discussed in the previous section, we identify the interval of the lunar wake passage by the value of N_i/N_{bg} and the value of $||V_i| - |V_{bg}||$, which are presented in Figures 2c and 2f, respectively. As TH-B passed the lunar wake, the value of N_i/N_{bg} reached a minimum of 0.28 and the value of $|V_i| - |V_{bg}|$ reached a minimum of −420 km/s, both under the threshold for the identification of a lunar wake passage, as marked by the orange horizontal dashed line (0.7 and −50 km/s). This result suggests that with this methodology, the interval of the lunar wake can be efficiently identified and excluded.

3.2 Statistical Comparison

Subsequently, we perform a statistical analysis based on a large amount of data over 6 years, from September 2011 to December 2017, to compare the two data sets, as presented in Figure 3. The original measurements are averaged by 10 minutes and plotted in each panel, with the *x*-axis for THEMIS and the *y*-axis for OMNI, respectively. The distributions of the measurements are plotted in color, indicating the total observational time in each pixel. The upper and lower rows are for TH-B and TH-C, respectively.

Comparisons of the *Y* and *Z* components of the magnetic field, B_y and B_z, between the measurement by THEMIS and the OMNI database are presented in Figures 3a–d. This comparison showed that the values of B_y and B_z from the two data sets are generally in good agreement without systemic deviation, that is, they are distributed evenly around the diagonal line marked by the red dashed lines. This result thus suggests that the magnetic field is highly consistent between the L1 point and near-Earth space.

Comparisons of the solar wind ion density N_i, velocity V_i, and dynamic pressure P_d between the THEMIS measurement and the OMNI database are presented in Figures 3e–j, as labeled in the figure. Unlike the magnetic field comparison, a systemic deviation is shown in the N_i data from the two data sets (Figures 3e and 3f), with higher N_i in the OMNI database in general, although the correlation coefficient is rather high, at a level of ~0.87. From

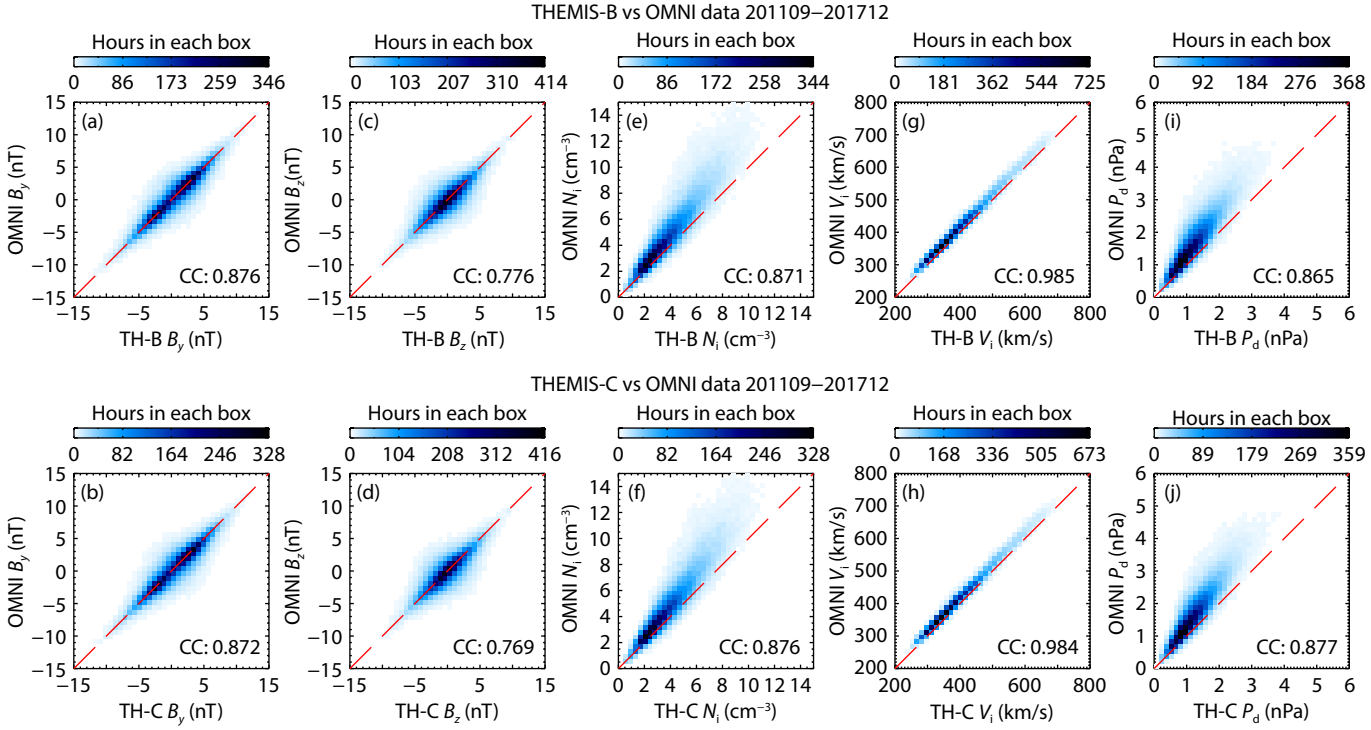

Figure 3. Comparison of (a–d) *Y* and *Z* components of the magnetic field, B_y and B_z, (e–f) solar wind ion number density N_i, (g–h) velocity V_i , and (i–j) dynamic pressure P_d between the OMNI database (*y*-axis) and THEMIS (TH) measurements (*x*-axis). The upper and lower rows are for TH-B and TH-C, respectively, and the color in each box represents the observation time.

Figures 3g and 3h, the deviation of the solar wind velocity is very small (less than 50 km/s) and negligible. The correlation coefficient is as high as ~0.98, suggesting that THEMIS measurements could be a good replacement for the solar wind velocity in the OMNI database. The dynamic pressure P_d, calculated with the information on density and velocity, inherits the deviation of N_i and V_i and thus has a similar signature as N_i. These deviations suggest that variation might be present in the solar wind environment as it propagates from the L1 point to near-Earth space.

3.3 Application of the Model Calculation to the Magnetopause Location

In this section, we show the use of solar wind data obtained at the L1 point (from the OMNI database) and in near-Earth space (from THEMIS measurements) as inputs to calculate the magnetopause location based on the empirical model by Shue et al. (1998), to examine the difference in inputs between the two data sets. We first present an example during the interplanetary shock event on August 31, 2017. As shown in Figure 4, this interplanetary shock was successively recorded in the OMNI database, which was originally obtained from measurements at the L1 point and observed by the TH-C spacecraft in near-Earth space (at $[X, Y] \sim [-29, 59]$ R_E in the Geocentric Solar Ecliptic coordinate). Note that all data presented in this figure have been interpolated by 2 minutes. In the OMNI observation, the dynamic pressure P_d increased from 5 to 12 nPa, and the Z component of the interplanetary magnetic field B_z varied gradually from 0 to 5 nT at 05:38 UT, as shown in Figure 4b, whereas in the TH-C measurement, P_d increased from 1.5 to 3.5 nPa, and the Z component of the interplanetary magnetic field B_z varied gradually from 0 to 5 nT at 05:42 UT, as shown in Figure 4e.

In the Earth's magnetosphere, TH-D was located near the subsolar magnetopause region at $[X, Y] \sim [9.8, -1.2]$ R_E in the Geocentric Solar Ecliptic coordinate at 05:36 UT, where the velocity of the anti-sunward plasma flow was observed to increase from ~50 km/s in the magnetosphere to ~100–160 km/s in the magnetosheath and then to ~390 km/s in the solar wind in 2 minutes, indicating a magnetopause crossing. This result thus suggests that before the arrival of the interplanetary shock, the radial distance of the subsolar magnetopause was approximately 10 R_E. The radial distances r_{MP} of the subsolar magnetopause are calculated based on the empirical model developed by Shue et al. (1998), with different measurements as the input parameters (see Figure 4). The r_{MP} calculated with the OMNI observation varies from 9.2 to 7.9 R_E, as shown in Figure 4c, whereas the r_{MP} calculated with the TH-C measurement varies from 10.7 to 9.5 R_E, as shown in Figure 4f. This result shows that the r_{MP} calculated with the TH-C measurement is more consistent with the TH-D observation than the OMNI observation.

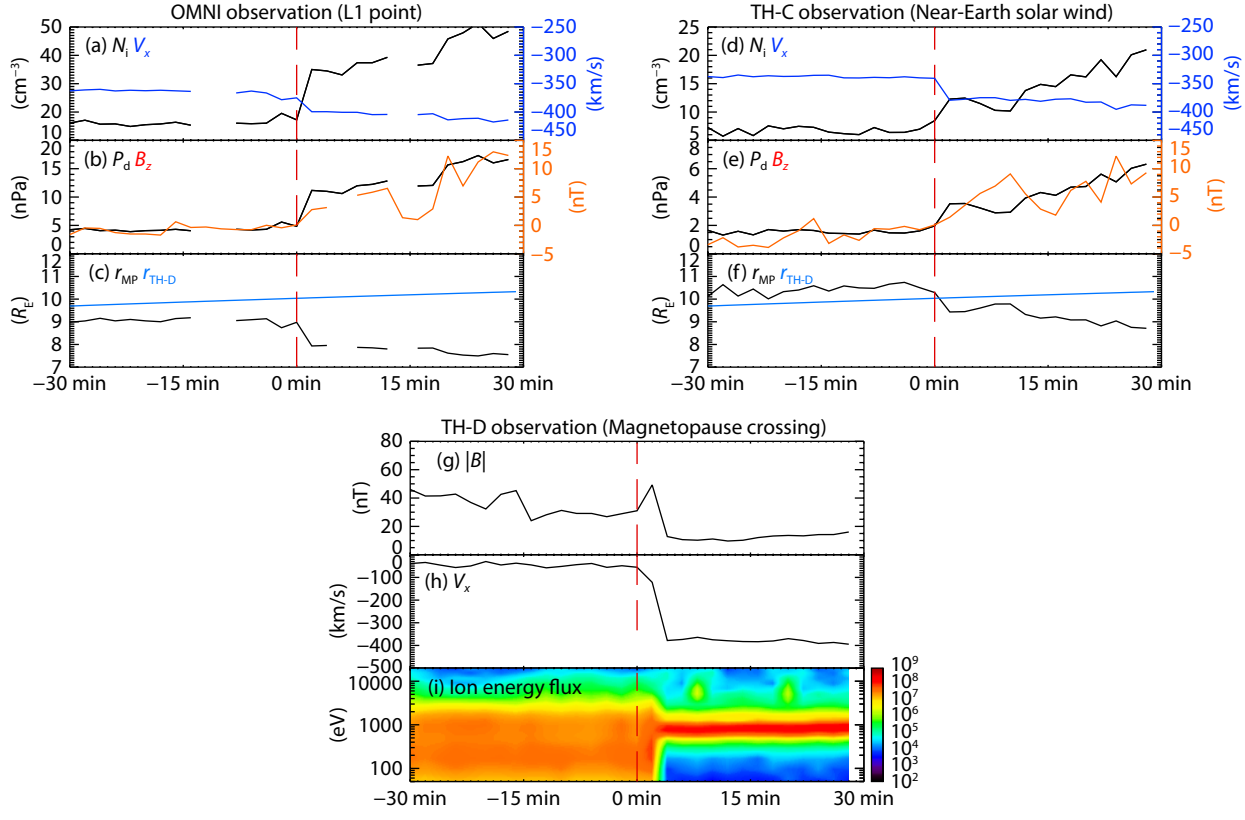

Figure 4. (a–b) Solar wind proton number density, X component of velocity, dynamic pressure, and Z component of the interplanetary magnetic field observed from the OMNI database. (c) The calculated radial distance of the magnetopause location based on the empirical model of Shue et al. (1998), shown as the black solid line, and the radial distance of THEMIS (TH)-D, shown as the blue dashed line. (d–f) The same format as (a–c) but with the TH-C measurement. (g–i) The magnetic field magnitude, X component of velocity, and ion energy flux measured by the TH-D spacecraft. The onset time of the interplanetary shock event observed by each probe is marked by the vertical dashed line.

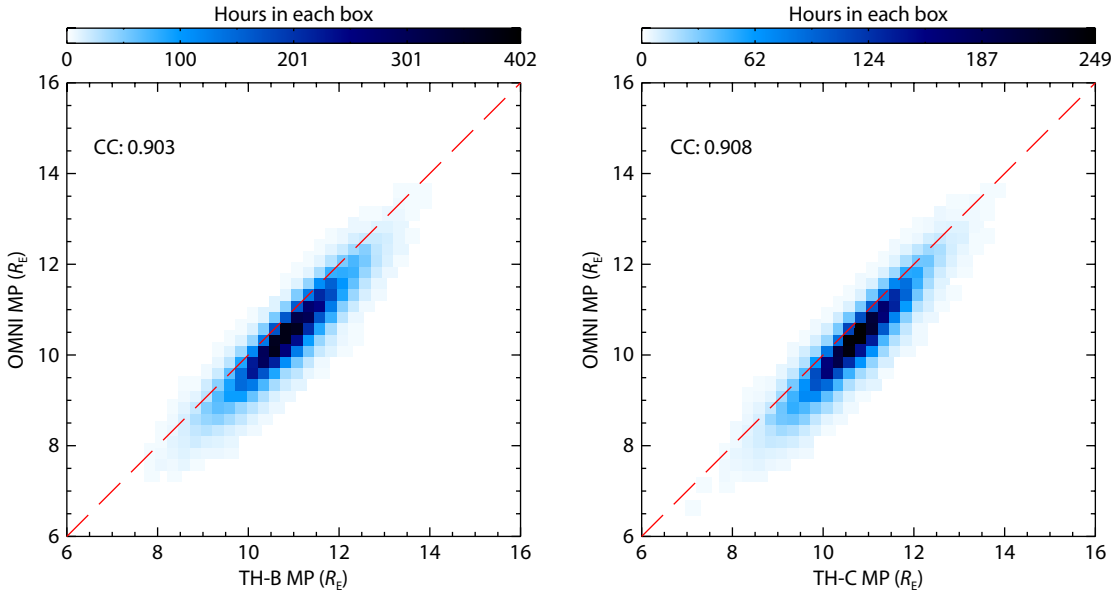

Figure 5. Comparison of the calculated radial distance of the subsolar magnetopause based on the empirical model of Shue et al. (1998), with input from the OMNI database and THEMIS (TH) measurements. The left and right panels are for TH-B and TH-C, respectively, and the color in each box represents the observation time.

Furthermore, a statistical comparison of the magnetopause calculated with THEMIS and OMNI data is performed for the time period from September 2011 to December 2017, as shown in Figure 5. Results of this comparison show that the r_{MP} calculated with THEMIS data is slightly larger than that calculated with OMNI data, within ~1.5–2 R_E in general.

3.4 Application of Quantification of the Magnetospheric Field Response to Interplanetary Shocks

A commonly observed feature in the response of the magnetosphere to the sudden compression of an interplanetary shock is an increase in the strength of the Earth's magnetic field, which can be quantitively described as an increase of the *SYM-H* index (Russell et al., 1994; Wang C et al., 2009, 2010). In this study, we investigate the variation in the *SYM-H* index during interplanetary shock events in the time period of September 2011 to December 2017 to compare different inputs of the solar wind measurements from the L1 point and near-Earth space. In total, 22 interplanetary shock events are identified in both the THEMIS (either TH-B or TH-C) and Wind spacecraft measurements, with the commonly used criteria defined by the parameters in the upstream and downstream regions (e.g., Kilpua et al., 2015): $B_{down}/B_{up} > 1.2$, $N_{down}/N_{up} > 1.2$, $T_{down}/T_{up} > 1.2$, and $V_{down} - V_{up} > 20$ km/s, where the time interval upstream is $t_{shock} - 9$ minutes to $t_{shock} - 1$ minute and downstream is $t_{shock} + 2$ minutes to $t_{shock} + 10$ minutes (t_{shock} is defined as the center of the jump of B). The values of t_{shock} for these interplanetary shock events identified by Wind and THEMIS are listed in Table 1.

Using these 22 interplanetary shock events, we perform a statistical investigation of the response of the global magnetospheric field strength (represented by the *SYM-H* index) to the interplanetary shock compression with THEMIS and Wind spacecraft measurements, as shown in Figures 6a and 6b, respectively. In each panel, the *y*-axis is the jump of the *SYM-H* index ($\Delta SYM\text{-}H$) and the *x*-axis is the enhancement of the square root of the dynamic pressure, $\Delta\sqrt{P_d}$. The relationship between $\Delta SYM\text{-}H$ and $\Delta\sqrt{P_d}$ can be linearly

Table 1. Interplanetary shocks' list shown in the statistics result in Figure 6.

Wind IPS onset time	THEMIS (B or C) IPS onset time
2017-10-24 07:56:27	2017-10-24 08:13:24
2017-08-31 04:35:45	2017-08-31 05:41:55
2016-04-14 06:56:51	2016-04-14 07:31:48
2016-03-11 04:29:12	2016-03-11 05:25:41
2015-12-14 12:41:15	2015-12-14 13:09:40
2015-09-20 05:23:21	2015-09-20 06:01:08
2015-06-21 16:04:18	2015-06-21 16:27:51
2015-03-11 04:21:18	2015-03-11 05:19:18
2015-01-26 07:52:03	2015-01-26 08:35:21
2014-07-06 10:07:18	2014-07-06 11:07:11
2014-06-23 22:15:57	2014-06-23 22:57:09
2014-05-03 16:37:51	2014-05-03 17:40:48
2013-10-29 09:33:46	2013-10-29 10:35:11
2013-09-02 01:56:51	2013-09-02 02:06:10
2013-07-09 20:11:39	2013-07-09 20:39:40
2013-05-18 00:19:57	2013-05-18 01:11:19
2013-04-13 22:13:15	2013-04-13 22:49:01
2012-07-20 04:08:30	2012-07-20 04:41:51
2012-06-16 09:03:33	2012-06-16 09:44:39
2012-03-12 08:29:15	2012-03-12 09:22:11
2011-11-28 21:00:09	2011-11-28 21:49:51
2011-09-26 11:44:18	2011-09-26 12:26:11

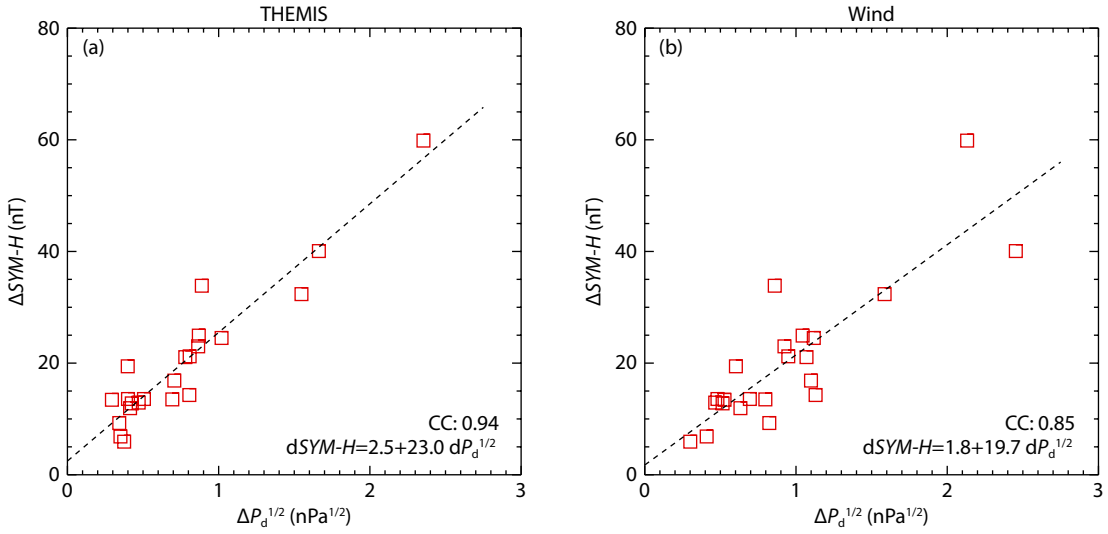

Figure 6. The $\Delta SYM\text{-}H$ is plotted versus $\Delta\sqrt{P_d}$ measured by THEMIS (a) and Wind (b) during the 22 interplanetary shock events. The squares denote the observations, and the solid line represents the fitted line.

fitted as $\Delta SYM\text{-}H = 2.5 + 23.0 \times \Delta\sqrt{P_d\,(\mathrm{THEMIS})}$ with a correlation coefficient of 0.94 for THEMIS in Figure 6a and $\Delta SYM\text{-}H = 1.8{+}19.7 \times \Delta\sqrt{P_d\,(\mathrm{Wind})}$, with a correlation coefficient of 0.85 for Wind in Figure 6b. Note that similar empirical relations have previously been given by Russell et al. (1994) with IMP-8 and ISEE-3 (International Sun–Earth Explorer-3) solar wind measurements at the L1 point ($\Delta SYM\text{-}H = 18.4 \times \Delta\sqrt{P_d}$) and by Wang C et al. (2010) with ACE solar wind measurements at the L1 point ($\Delta SYM\text{-}H = 18.01 \times \Delta\sqrt{P_d}$). Our results in Figure 6b are quite consistent with those of previous work because they are all based on the L1 point measurement. However, the higher correlation coefficient and higher slope in Figure 6a would result from the lower P_d measured in near-Earth space, as presented in Figures 3i and 3j, suggesting that such measurements could be useful for better understanding the interaction between the solar wind and the magnetosphere.

4. Conclusions

We perform a systematic validation of THEMIS measurements as a solar wind monitor and compare them with data obtained from the L1 point, including OMNI and Wind measurements. Our conclusions are as follows:

(1) The *Y* and *Z* components of the magnetic field and flow speed are generally consistent between the THEMIS and OMNI data sets.
(2) The proton number density and dynamic pressure measured by THEMIS are generally lower than those obtained from OMNI data, suggesting a possible variation in the solar wind environment during propagation from the L1 point to near-Earth space.
(3) The solar wind data from THEMIS measurements and OMNI data during an interplanetary shock compression that occurred on August 31, 2017, are input into the empirical magnetopause model developed by Shue et al. (1998). The calculated magnetopause location based on the TH-C measurement is more consistent with the location of TH-D near the subsolar region crossing the magnetopause.
(4) The correlations between $\Delta SYM\text{-}H$ and $\Delta\sqrt{P_d}$ during 22 interplanetary shocks are calculated with THEMIS and Wind data, respectively. The correlation coefficient is higher for THEMIS, suggesting that solar wind measurements in near-Earth space could be useful for better understanding the solar wind–magnetosphere interaction.

Acknowledgments

This work was supported by the National Natural Science Foundation of China (grants 41821003 and 41974194). We thank the fluxgate magnetometer and electrostatic analyzer teams of the THEMIS mission, the solar wind experiment and magnetic field instrument teams of the Wind mission, and the OMNI team for making these data available.

References

Angelopoulos, V., Sibeck, D., Carlson, C. W., McFadden, J. P., Larson, D., Lin, R. P., Bonnell, J. W., Mozer, F. S., Ergun, R., … Sigwarth, J. (2008). First results from the THEMIS mission. *Space Sci. Rev.*, *141*(1–4), 453–476. https://doi.org/10.1007/s11214-008-9378-4

Angelopoulos, V. (2011). The ARTEMIS mission. *Space Sci. Rev.*, *165*(1), 3–25. https://doi.org/10.1007/s11214-010-9687-2

Auster, H. U., Glassmeier, K. H., Magnes, W., Aydogar, O., Baumjohann, W., Constantinescu, D., Fischer, D., Fornacon, K. H., Georgescu, E., … Wiedemann, M. (2008). The THEMIS fluxgate magnetometer. *Space Sci. Rev.*, *141*(1–4), 235–264. https://doi.org/10.1007/s11214-008-9365-9

Borovsky, J. E., and Denton, M. H. (2006). Differences between CME-driven storms and CIR-driven storms. *J. Geophys. Res.: Space Phys.*, *111*(A7), A07S08. https://doi.org/10.1029/2005JA011447

Bruno, R., Carbone, V., Sorriso-Valvo, L., and Bavassano, B. (2003). Radial evolution of solar wind intermittency in the inner heliosphere. *J. Geophys. Res.: Space Phys.*, *108*(A3), 1130. https://doi.org/10.1029/2002JA009615

Cao, J. B., Duan, J. T., Du, A. M., Ma, Y. D., Liu, Z. X., Zhou, G. C., Yang, D. M., Zhang, T. L., Li, X. L., … Li, Q. (2008). Characteristics of middle- to low-latitude Pi2 excited by bursty bulk flows. *J. Geophys. Res.: Space Phys.*, *113*(A7), A07S15. https://doi.org/10.1029/2007JA012629

Cao, J. B., Yan, C. X., Dunlop, M., Reme, H., Dandouras, I., Zhang, T. L., Yang, D. M., Moiseyev, A., Solovyev, S. I., … Mishin, V. (2010). Geomagnetic signatures of current wedge produced by fast flows in a plasma sheet. *J. Geophys. Res.: Space Phys.*, *115*(A8), A08205. https://doi.org/10.1029/2009JA014891

Foster, J. C., Wygant, J. R., Hudson, M. K., Boyd, A. J., Baker, D. N., Erickson, P. J., and Spence, H. E. (2015). Shock-induced prompt relativistic electron

acceleration in the inner magnetosphere. *J. Geophys. Res.*: *Space Phys.*, *120*(3), 1661–1674. https://doi.org/10.1002/2014JA020642

Fu, H. S., Cao, J. B., Mozer, F. S., Lu, H. Y., and Yang, B. (2012). Chorus intensification in response to interplanetary shock. *J. Geophys. Res.*: *Space Phys.*, *117*(A1), A01203. https://doi.org/10.1029/2011JA016913

Fu, H. S., Cao, J. B., Khotyaintsev, Y. V., Sitnov, M. I., Runov, A., Fu, S. Y., Hamrin, M., André, M., Retinò, A., … Huang, S. Y. (2013). Dipolarization fronts as a consequence of transient reconnection: in situ evidence. *Geophys. Res. Lett.*, *40*(23), 6023–6027. https://doi.org/10.1002/2013GL058620

Halekas, J. S., Angelopoulos, V., Sibeck, D. G., Khurana, K. K., Russell, C. T., Delory, G. T., Farrell, W. M., McFadden, J. P., Bonnell, J. W., … Glassmeier, K. H. (2011). First results from ARTEMIS, a new two-spacecraft lunar mission: counter-streaming plasma populations in the lunar wake. *Space Sci. Rev.*, *165*(1–4), 93–107. https://doi.org/10.1007/s11214-010-9738-8

Kanekal, S. G., Baker, D. N., Fennell, J. F., Jones, A., Schiller, Q., Richardson, I. G., Li, X., Turner, D. L., Califf, S., … Wygant, J. R. (2016). Prompt acceleration of magnetospheric electrons to ultrarelativistic energies by the 17 March 2015 interplanetary shock. *J. Geophys. Res.*: *Space Phys.*, *121*(8), 7622–7635. https://doi.org/10.1002/2016JA022596

Kilpua, E. K. J., Lumme, E., Andreeova, K., Isavnin, A., and Koskinen, H. E. J. (2015). Properties and drivers of fast interplanetary shocks near the orbit of the Earth (1995–2013). *J. Geophys. Res.*: *Space Phys.*, *120*(6), 4112–4125. https://doi.org/10.1002/2015JA021138

Korotova, G., Sibeck, D., Thaller, S., Wygant, J., Spence, H., Kletzing, C., Angelopoulos, V., and Redmon, R. (2018). Multisatellite observations of the magnetosphere response to changes in the solar wind and interplanetary magnetic field. *Ann. Geophys.*, *36*(5), 1319–1333. https://doi.org/10.5194/angeo-36-1319-2018

Lepping, R. P., Acũna, M. H., Burlaga, L. F., Farrell, W. M., Slavin, J. A., Schatten, K. H., Mariani, F., Ness, N. F., Neubauer, F. M., … Worley, E. M. (1995). The WIND magnetic field investigation. *Space Sci. Rev.*, *71*(1–4), 207–229. https://doi.org/10.1007/BF00751330

Li, L. Y., Yu, J., Cao, J. B., and Yuan, Z. G. (2016). Compression-amplified EMIC waves and their effects on relativistic electrons. *Phys. Plasmas*, *23*(6), 062116. https://doi.org/10.1063/1.4953899

Li, X. L., Roth, I., Temerin, M., Wygant, J. R., Hudson, M. K., and Blake, J. B. (1993). Simulation of the prompt energization and transport of radiation belt particles during the March 24, 1991 SSC. *Geophys. Res. Lett.*, *20*(22), 2423–2426. https://doi.org/10.1029/93GL02701

Liu, W., Sarris, T. E., Li, X., Ergun, R., Angelopoulos, V., Bonnell, J., and Glassmeier, K. H. (2010). Solar wind influence on Pc4 and Pc5 ULF wave activity in the inner magnetosphere. *J. Geophys. Res.*: *Space Phys.*, *115*(A12), A12201. https://doi.org/10.1029/2010JA015299

Liu, W., Cao, J. B., Li, X., Sarris, T. E., Zong, Q. G., Hartinger, M., Takahashi, K., Zhang, H., Shi, Q. Q., and Angelopoulos, V. (2013). Poloidal ULF wave observed in the plasmasphere boundary layer. *J. Geophys. Res.*: *Space Phys.*, *118*(7), 4298–4307. https://doi.org/10.1002/jgra.50427

Liu, W. L., Li, X., Sarris, T., Cully, C., Ergun, R., Angelopoulos, V., Larson, D., Keiling, A., Glassmeier, K. H., and Auster, H. U. (2009). Observation and modeling of the injection observed by THEMIS and LANL satellites during the 23 March 2007 substorm event. *J. Geophys. Res.*: *Space Phys.*, *114*(A1), A00C18. https://doi.org/10.1029/2008JA013498

Liu, W. L., Tu, W. C., Li, X. L., Sarris, T., Khotyaintsev, Y., Fu, H. S., Zhang, H., and Shi, Q. Q. (2016). On the calculation of electric diffusion coefficient of radiation belt electrons with in situ electric field measurements by THEMIS. *Geophys. Res. Lett.*, *43*(3), 1023–1030. https://doi.org/10.1002/2015GL067398

Liu, Y., Zong, Q. G., Zhou, X. Z., Hao, Y. X., and Liu, Z. Y. (2019). Understanding electron dropout echoes induced by interplanetary shocks: test particle simulations. *J. Geophys. Res.*: *Space Phys.*, *124*(8), 6759–6775. https://doi.org/10.1029/2019JA027018

Liu, Z. Y., Zong, Q. G., Hao, Y. X., Zhou, X. Z., Ma, X. H., and Liu, Y. (2017). Electron dropout echoes induced by interplanetary shock: a statistical study. *J. Geophys. Res.*: *Space Phys.*, *122*(8), 8037–8050. https://doi.org/10.1002/2017JA024045

McFadden, J. P., Carlson, C. W., Larson, D., Ludlam, M., Abiad, R., Elliott, B., Turin, P., Marckwordt, M., and Angelopoulos, V. (2008). The THEMIS ESA plasma instrument and in-flight calibration. *Space Sci. Rev.*, *141*(1–4), 277–302. https://doi.org/10.1007/s11214-008-9440-2

Ogilvie, K. W., Chornay, D. J., Fritzenreiter, R. J., Hunsaker, F., Keller, J., Lobell, J., Miller, G., Scudder, J. D., Sittler, E. C., … Gergin, E. (1995). SWE, a comprehensive plasma instrument for the WIND spacecraft. *Space Sci. Rev.*, *71*(1–4), 55–77. https://doi.org/10.1007/BF00751326

Patel, M., Li, Z., Hudson, M., Claudepierre, S., and Wygant, J. (2019). Simulation of prompt acceleration of radiation belt electrons during the 16 July 2017 storm. *Geophys. Res. Lett.*, *46*(13), 7222–7229. https://doi.org/10.1029/2019GL083257

Richardson, J. D., Paularena, K. I., Lazarus, A. J., and Belcher, J. W. (1995). Radial evolution of the solar wind from IMP 8 to Voyager 2. *Geophys. Res. Lett.*, *22*(4), 325–328. https://doi.org/10.1029/94GL03273

Russell, C. T., Ginskey, M., and Petrinec, S. M. (1994). Sudden impulses at low-latitude stations: steady state response for northward interplanetary magnetic field. *J. Geophys. Res.*: *Space Phys.*, *99*(A1), 253–261. https://doi.org/10.1029/93ja02288

Shen, X. C., Zong, Q. G., Shi, Q. Q., Tian, A. M., Sun, W. J., Wang, Y. F., Zhou, X. Z., Fu, S. Y., Hartinger, M. D., and Angelopoulos, V. (2015). Magnetospheric ULF waves with increasing amplitude related to solar wind dynamic pressure changes: the time history of events and macroscale interactions during substorms (THEMIS) observations. *J. Geophys. Res.*: *Space Phys.*, *120*(9), 7179–7190. https://doi.org/10.1002/2014JA020913

Shen, X. C., Hudson, M. K., Jaynes, A. N., Shi, Q. Q., Tian, A. M., Claudepierre, S. G., Qin, M. R., Zong, Q. G., and Sun, W. J. (2017). Statistical study of the storm time radiation belt evolution during Van Allen Probes era: CME- versus CIR-driven storms. *J. Geophys. Res.*: *Space Phys.*, *122*(8), 8327–8339. https://doi.org/10.1002/2017JA024100

Shue, J. H., Song, P., Russell, C. T., Steinberg, J. T., Chao, J. K., Zastenker, G., Vaisberg, O. L., Kokubun, S., Singer, H. J., … Kawano, H. (1998). Magnetopause location under extreme solar wind conditions. *J. Geophys. Res.*: *Space Phys.*, *103*(A8), 17691–17700. https://doi.org/10.1029/98JA01103

Tang, C. L., Wang, X., Ni, B. B., Su, Z. P., and Zhang, J. C. (2022). The 600 keV electron injections in the Earth's outer radiation belt: A statistical study. *Earth Planet. Phys.*, *6*(2), 149–160. https://doi.org/10.26464/epp2022012

Wang, C., Liu, J. B., Li, H., Huang, Z. H., Richardson, J. D., and Kan, J. R. (2009). Geospace magnetic field responses to interplanetary shocks. *J. Geophys. Res.*: *Space Phys.*, *114*(A5), A05211. https://doi.org/10.1029/2008JA013794

Wang, C., Li, H., Richardson, J. D., and Kan, J. R. (2010). Interplanetary shock characteristics and associated geosynchronous magnetic field variations estimated from sudden impulses observed on the ground. *J. Geophys. Res.*: *Space Phys.*, *115*(A9), A09215. https://doi.org/10.1029/2009JA014833

Wang, C. R., Rankin, R., and Zong, Q. G. (2015). Fast damping of ultralow frequency waves excited by interplanetary shocks in the magnetosphere. *J. Geophys. Res.*: *Space Phys.*, *120*(4), 2438–2451. https://doi.org/10.1002/2014JA020761

Wei, Y., Hong, M. H., Wan, W. X., Du, A. M., Lei, J. H., Zhao, B. Q., Wang, W. B., Ren, Z. P., and Yue, X. A. (2008). Unusually long lasting multiple penetration of interplanetary electric field to equatorial ionosphere under oscillating IMF B_z. *Geophys. Res. Lett.*, *35*(2), L02102. https://doi.org/10.1029/2007GL032305

Wei, Y., Pu, Z., Hong, M., Zong, Q., Ren, Z., Fu, S., Xie, L., Alex, S., Cao, X., … Chu, X. (2009). Westward ionospheric electric field perturbations on the dayside associated with substorm processes. *J. Geophys. Res.*: *Space Phys.*, *114*(A12), A12209. https://doi.org/10.1029/2009JA014445

Weimer, D. R., and King, J. H. (2008). Improved calculations of interplanetary magnetic field phase front angles and propagation time delays. *J. Geophys. Res.*: *Space Phys.*, *113*(A1), A01105. https://doi.org/10.1029/2007JA012452

Xiong, Y., Xie, L., Fu, S. Y., Ni, B. B., and Pu, Z. Y. (2021). Non-storm erosion of MeV electron outer radiation belt down to L^* < 4.0 associated with successive enhancements of solar wind density. *Earth Planet. Phys.*, *5*(6), 581–591. https://doi.org/10.26464/epp2021051

Yu, Y. Q., and Ridley, A. J. (2011). Understanding the response of the ionosphere–magnetosphere system to sudden solar wind density increases. *J. Geophys. Res.*: *Space Phys.*, *116*(A4), A04210. https://doi.org/10.1029/2010JA015871

Yu, Y. Q., Cao, J. B., Fu, H. S., Lu, H. Y., and Yao, Z. H. (2017). The effects of bursty bulk flows on global-scale current systems. *J. Geophys. Res.*: *Space Phys.*, *122*(6), 6139–6149. https://doi.org/10.1002/2017JA024168

Yue, C., Zong, Q. G., Zhang, H., Wang, Y. F., Yuan, C. J., Pu, Z. Y., Fu, S. Y., Lui, A. T. Y., Yang, B., and Wang, C. R. (2010). Geomagnetic activity triggered by interplanetary shocks. *J. Geophys. Res.*: *Space Phys.*, *115*(A5), A00I05. https://doi.org/10.1029/2010JA015356

Zhang, D. J., Liu, W. L., Li, X. L., Sarris, T., Xiao, C., and Wygant, J. R. (2018). Observations of impulsive electric fields induced by interplanetary shock. *Geophys. Res. Lett.*, *45*(15), 7287–7296. https://doi.org/10.1029/2018GL078809

Zhang, D. J., Liu, W. L., Li, X. L., Sarris, T. E., Wang, Y. F., Xiao, C., Zhang, Z., and Wygant, J. R. (2020). Relation between shock-related impulse and subsequent ULF wave in the earth's magnetosphere. *Geophys. Res. Lett.*, *47*(23), e2020GL090027. https://doi.org/10.1029/2020GL090027

Zhang, H., Khurana, K. K., Kivelson, M. G., Angelopoulos, V., Wan, W. X., Liu, L. B., Zong, Q. G., Pu, Z. Y., Shi, Q. Q., and Liu, W. L. (2014). Three-dimensional lunar wake reconstructed from ARTEMIS data. *J. Geophys. Res.*: *Space Phys.*, *119*(7), 5220–5243. https://doi.org/10.1002/2014JA020111

Zhang, X. Y., Zong, Q. G., Wang, Y. F., Zhang, H., Xie, L., Fu, S. Y., Yuan, C. J., Yue, C., Yang, B., and Pu, Z. Y. (2010). ULF waves excited by negative/positive solar wind dynamic pressure impulses at geosynchronous orbit. *J. Geophys. Res.*: *Space Phys.*, *115*(A10), A10221. https://doi.org/10.1029/2009JA015016

Zhou, X. Y., and Tsurutani, B. T. (1999). Rapid intensification and propagation of the dayside aurora: large scale interplanetary pressure pulses (fast shocks). *Geophys. Res. Lett.*, *26*(8), 1097–1100. https://doi.org/10.1029/1999GL900173

Zhou, X. Y., Haerendel, G., Moen, J. I., Trondsen, E., Clausen, L., Strangeway, R. J., Lybekk, B., and Lorentzen, D. A. (2017). Shock aurora: Field-aligned discrete structures moving along the dawnside oval. *J. Geophys. Res.*: *Space Phys.*, *122*(3), 3145–3162. https://doi.org/10.1002/2016JA022666

Zhu, M. H., Yu, Y. Q., Cao, X., Ni, B. B., Tian, X. B., Cao, J. B., and Jordanova, V. K. (2022). Effects of polarization-reversed electromagnetic ion cyclotron waves on the ring current dynamics. *Earth Planet. Phys.*, *6*(4), 329–338. https://doi.org/10.26464/epp2022037

Zong, Q. G., Zhou, X. Z., Wang, Y. F., Li, X., Song, P., Baker, D. N., Fritz, T. A., Daly, P. W., Dunlop, M., and Pedersen, A. (2009). Energetic electron response to ULF waves induced by interplanetary shocks in the outer radiation belt. *J. Geophys. Res.*: *Space Phys.*, *114*(A10), A10204. https://doi.org/10.1029/2009JA014393